crystals

MDPI

Review

Oxidative Coupling of Methane: Perspective for High-Value C_2 Chemicals

Palle Ramana Murthy †, Yang Liu †, Guohao Wu, Yanan Diao and Chuan Shi *

State Key Laboratory of Fine Chemicals, College of Chemical Engineering, Dalian University of Technology, Dalian 116024, China; ramanapalle@dlut.edu.cn (P.R.M.); 18842687020@163.com (Y.L.); 18340878859@163.com (G.W.); d891497031@163.com (Y.D.)

* Correspondence: chuanshi@dlut.edu.cn

† These authors contributed equally.

Abstract: The oxidative coupling of methane (OCM) to C_2 hydrocarbons (C_2H_4 and C_2H_6) has aroused worldwide interest over the past decade due to the rise of vast new shale gas resources. However, obtaining higher C_2 selectivity can be very challenging in a typical OCM process in the presence of easily oxidized products such as C_2H_4 and C_2H_6. Regarding this, different types of catalysts have been studied to achieve desirable C_2 yields. In this review, we briefly presented three typical types of catalysts such as alkali/alkaline earth metal doped/supported on metal oxide catalysts (mainly for Li doped/supported catalysts), modified transition metal oxide catalysts, and pyrochlore catalysts for OCM and highlighted the features that play key roles in the OCM reactions such as active oxygen species, the mobility of the lattice oxygen and surface alkalinity of the catalysts. In particular, we focused on the pyrochlore ($A_2B_2O_7$) materials because of their promising properties such as high melting points, thermal stability, surface alkalinity and tunable M-O bonding for OCM reaction.

Keywords: oxidative coupling of methane; ethylene; lattice oxygen; pyrochlore; $La_2Ce_2O_7$

check for updates

Citation: Murthy, P.R.; Liu, Y.; Wu, G.; Diao, Y.; Shi, C. Oxidative Coupling of Methane: Perspective for High-Value C_2 Chemicals. *Crystals* **2021**, *11*, 1011. https://doi.org/10.3390/cryst11091011

Academic Editors: Wenping Ma and Ajay K. Dalai

Received: 19 July 2021
Accepted: 20 August 2021
Published: 24 August 2021

1. Introduction

Methane, being an abundant hydrocarbon resource, provides a kind of comparably cheaper and environmentally friendly fuel [1,2]. The use of natural gas as an important industrial feedstock has increased as compared to petroleum over the past few decades due to the extraction of natural gas from unconventional sources, for example shale deposits [3]. Figure 1 reveals the recoverable shale gas reserves in the world in trillion cubic feet (TCF).

Ethylene is used as a raw material in the manufacture of polymers such as polyethylene, polystyrene, polyvinyl chloride and polyethylene terephthalate, as well as fibers, petrochemical products and organic chemicals. It is also used as the main feedstock (~50%) in the chemical industry. Hence, many global chemical companies are planning to develop economical and feasible processes to produce ethylene directly from methane [3,4].

In general, steam and the thermal cracking of naphtha processes are used for ethylene production in petroleum refineries. Global ethylene production is mainly dependent on these processes [5,6]. However, some of the key problems identified here are energy intensiveness (up to 40 GJ heat per tonne ethylene) and environmental unsustainability [7]. High temperatures (>1200 °C) are required for breaking the C-H bond (bond energy, 440 kJ/mol) in this process and approximately three tons of CO_2 is released per ton of ethylene production [8]. Therefore, another way ethylene can be produced from natural gas is via indirect paths by the formation of syngas (CO/H_2) through the catalytic Fischer-Tropsch synthesis (FTS) process [9,10]. Alternatively, syngas can be transformed into methanol and then methanol to ethylene [11,12]. In addition to this, methane can also be converted directly to value-added chemicals and fuels through oxidative and non-oxidative catalytic reaction pathways. The non-oxidative processes involve the coupling of

methane to olefins; this process suffers from intrinsic thermodynamic limitations and needs higher energy for large-scale applications [13]. Therefore, most of the research for direct conversion has emphasized a process called oxidative coupling of methane (OCM) [14–19].

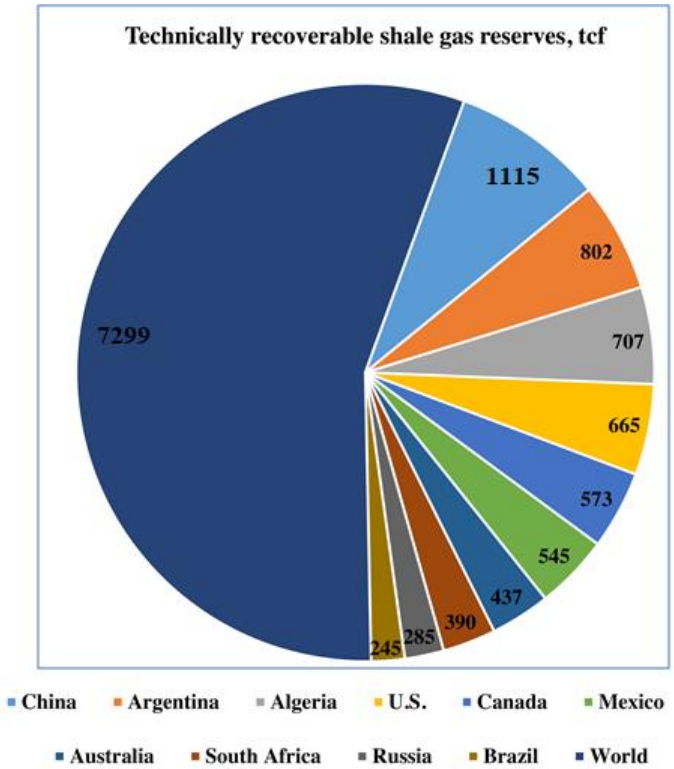

Figure 1. Global projection of technically recoverable shale gas reserves in trillion cubic feet (TCF). The leading global countries are shown in different colors. Reproduced with permission from [3] Copyright 2016 Elsevier.

Zhao et al. [14] prepared hierarchically structured porous flower-like materials such as La_2O_3-H- and Sr-doped ($Sr_{0.1}LaO_x$-H) compounds and highly dense non-porous (La_2O_3-D and $Sr_{0.1}LaO_x$-D) microspheres. The porous materials showed higher catalytic performances in OCM than non-porous catalysts, presumably due to the creation of the active sites in porous materials, which could enhance the activation of oxygen. $Sr_{0.1}LaO_x$-H showed better OCM results than La_2O_3-H and reached the optimum selectivity (~48%) and C_2 yield (~19%) at 550 °C due to Sr isolating the active sites of the catalyst, which can act as a strong basic site. However, deactivation occurred in the $Sr_{0.1}LaO_x$-H catalyst during OCM in ~30 h, but adding a small amount of Zr can produce better stability in OCM. Lopes et al. [15] prepared $La_2Ti_2O_7$-based catalysts ($LaTi_{1-x}Mg_xO_{3+\delta}$) with varied Ti/Mg molar ratios through the partial substitution of Ti by Mg to regulate the quantities of alkaline sites and surface oxygen species, properties crucial for OCM reaction. The characterization data testifies that alkalinity and the surface oxygen vacancy concentration increase as Mg increases. The presence of high amounts of Mg on the surface can increase the incidence of defective sites in the interface formed by La-O-Mg. In general, the rich defects are active and selective toward C_2 production in the OCM reaction. Hence, the catalytic results showed that methane conversion and C_2 selectivity increased as a function of the Mg amount, and also this catalyst exhibited high thermal stability after 24 h on stream. Sato et al. [16] proposed that, in the presence of an electric field, the $CePO_4$ nanorod catalysts showed high activity and stability even at low temperatures for OCM (C_2 yield = 18%) without any external heating. Because, in the electric field, these catalysts can be produced and regenerate the surface-active oxygen species even at low temperatures, which are mainly responsible for OCM, Schmack et al. proposed a meta-analysis method. It is often useful ascertain the links between a catalyst's physicochemical characteristics and its performance

in an OCM reaction [17]. Pirro et al. [18] proposed the process simulator and illustrated it for the OCM to determine the catalyst-dependent kinetics for industrial implementation. For the case study, the feeding of oxygen and cooling were operated under a multi-stage adiabatic configuration. Three catalysts (Sn-Li/MgO, NaMnW/SiO_2 and Sr/La_2O_3) were introduced to estimate the methane conversion and C_{2+} yield compared to a single stage. They revealed that multi-phase configuration is advantageous compared to a single phase.

The OCM process follows the value-added transformation of natural gas through the catalytic reaction between methane and oxygen for ethylene production. Although more than four decades have passed since the initial work on OCM, this reaction has still not been able to be used as a successful industrial process for ethylene production because of the lower yield (<30%) of C_2 products.

In the reaction mechanism of OCM, the first step of abstraction of a hydrogen atom from methane with the help of surface-active oxygen results in the formation of hydroxyl groups, which react with each other to produce H_2O, and at the same time create an oxygen vacancy on the catalyst surface. Meanwhile, methyl radicals will combine to form ethane which further undergoes a dehydrogenation reaction to produce the desired product of ethylene, as shown in Figure 2. According to previous reports, active oxygen species on the surface of catalyst consist of peroxide (O_2^{2-}), lattice oxygen (O^{2-}), carbonate (CO_3^{2-}), superoxide (O_2^-) and hydroxide (OH^-) ions. Among all, surface lattice oxygen (O^{2-}) anions play a crucial role in attaining the C_2 product selectively, whereas surface electrophilic anions (O^-, O_2^- and O_2^{2-}) usually result in an over-oxidation of the CO_x product [20,21].

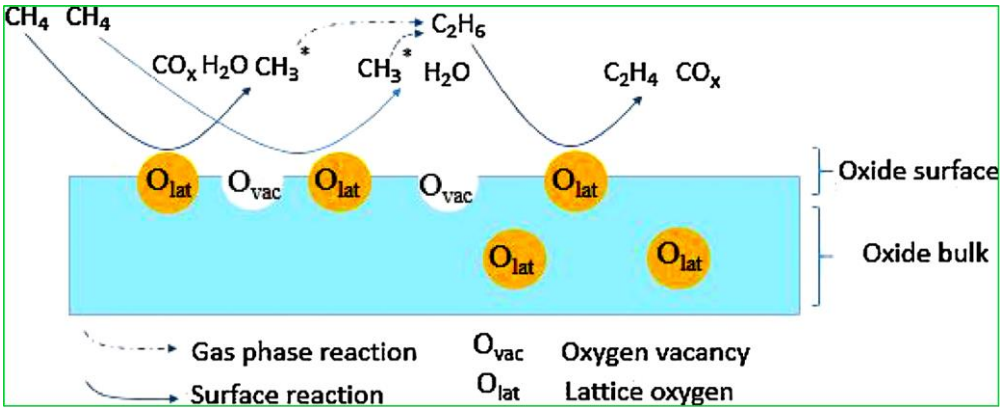

Figure 2. Diagrammatic representation of oxidative coupling of methane (OCM) reaction on a metal oxide catalyst surface. Reproduced with permission from [19]. Copyright 2018 Elsevier.

From the pioneering work of Keller and Bhasin [22] and Ito and Lunsford [23], various catalysts have been investigated to attain adequate methane conversion and C_2 selectivity/yield. Most of the metal oxides in the periodic table, such as transition metal oxides, rare earth metal oxides, alkali or alkaline earth metal oxides, perovskites and pyrochlore compounds, have been individually or in various combinations tested for OCM reaction [3,24–28]. Zavyalova et al. [29] conducted a comprehensive statistical analysis of about ~1000 research articles related to OCM. They pointed out that both rare-earth metal oxides and alkaline-earth metal oxides, along with alkali metal oxides, are good candidates for OCM reaction. In addition, binary and ternary combinations of metal oxides are also crucial for high and sustainable catalytic activity in the OCM reaction. The selectivity of the catalysts can be further improved by using various dopants such as alkali (Cs, Na) and alkaline earth (Sr, Ba) metals, whereas Mn, W and the Cl^- anion dopants can be used to enhance the catalytic activity. Figure 3 represents the most promising OCM catalytic systems with C_2 yields greater than 25%.

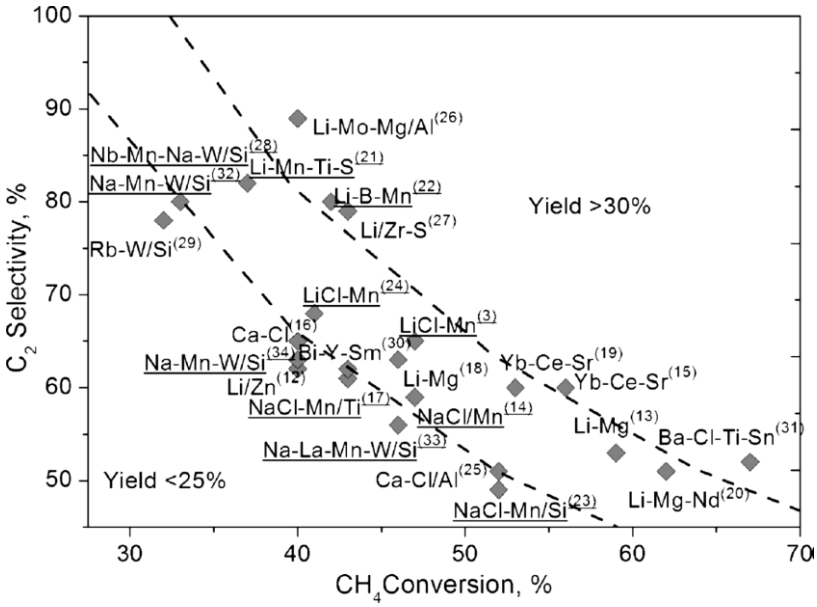

Figure 3. Various OCM catalysts with C_2 yields (≥25%). Reproduced with permission from [29]. Copyright 2011 Wiley-VCH.

This review presents three types of catalysts for OCM reaction and highlights the features that play key roles in the OCM reactions, such as active oxygen species, the mobility of the lattice oxygen, and the surface alkalinity of the catalysts. The catalyst compositions and their catalytic functions are also discussed. Special attention has been focused on pyrochlore ($A_2B_2O_7$) materials with promising properties such as high melting points, thermal stability, surface alkalinity and tunable M-O bonding, these being essential for OCM reaction.

2. Catalysts for Oxidative Coupling of Methane

Oxide catalysts are the main catalysts used for OCM reaction. These can be a pristine form or modified with group alkali/alkaline earth metals or transitional metals. These catalytic systems are established under various synthesis methods such as hydrothermal, sol-gel, precipitation, impregnation, thermal decomposition and flame spray pyrolysis to yield tunable catalyst compositions by varying basicity and oxygen vacancies, which are the most important characteristics of OCM catalysts and also key factors in activating methane. These catalysts can be coupled with tunable reaction conditions such as space, velocity and temperature to enhance methane conversion, selectivity and yield [19,30].

2.1. Alkali/Alkaline Earth Metal Doped/Supported on Metal Oxide Catalysts

Pristine or unmodified metal oxide catalysts generally exhibit low C_2 selectivity/yield and rapid deactivation in OCM reaction. Modified systems are considered to achieve higher yield at lower temperature regions due to the altered either basicity or oxygen vacancies and/or other defects, which are crucial for CH_4 activation [31–36]. Ferreira et al. [32] developed CeO_2 catalysts modified with earth alkaline metals (M = Mg, Ca, and Sr) and demonstrated that among these three dopants, Ca-doped CeO_2 catalyst showed the best performance in the OCM reaction. This is mainly due to the similar ionic radii of Ca^{2+} and Ce^{4+} ions and the higher ratio of the oxygen species O_2^- and O_2^{2-} to lattice oxygen and a high amount of surface basic sites. Yıldız et al. [33] proved that mesoporous TiO_2-rutile supported Mn_xO_y-Na_2WO_4 catalysts' better performance than commercial TiO_2-rutile- and TiO_2-anatase-supported catalysts. In addition, this catalyst is stable during 16 h on stream in OCM. Ivanov et al. [34] synthesized Mg, Al, Ca, Ba and Pb-substituted titanates $SrTi_{1-x}A_xO_3$(A = Mg, Al, Ca, Ba, Pb, x = 0.1) and $Sr_2Ti_{1-x}A_xO_4$(A = Mg, Al, x = 0.1) catalysts by using a mechanochemical method and tested these catalysts for OCM reaction

at 850 and 900 °C. Finally, they demonstrated that among these dopants, Mg- and Al-doped $SrTiO_3$ and Sr_2TiO_4 catalysts showed the best performance in the OCM reaction to provide a higher C_2 yield up to 25% and C_2 selectivity around 66%, presumably due to (Sr, Mg)O oxide segregate on the surface, which has active oxygen ion-radicals. Peng et al. [35] developed SnO_2 modified with alkaline metals and demonstrated that the Li-doped SnO_2 catalyst showed the best performance in the OCM reaction among these dopants. This is mainly due to the higher surface intermediate alkaline sites and electrophilic oxygen species. Moreover, this catalyst showed stable catalytic performance up to 100 h without deactivation. Finally, they proposed that the catalytic activity and selectivity towards the desired products were higher for the optimized catalyst (Sn_5Li_5) than Mn-Na_2WO_4/SiO_2 at a lower temperature (750 °C), which is considered a state-of-the-art catalyst for OCM. Kim et al. [37] carefully explored the role of oxygen species using lanthanum-based perovskite catalysts, which are prepared by a citrate sol-gel method. Their study found that the active surface lattice oxygen species and a facile filling of lattice oxygen vacancies by gas-phase oxygen are responsible for the production of C_2 hydrocarbons in OCM.

Elkins et al. [38] studied rare earth oxides (Sm_2O_3, TbO_x, PrO_y and CeO_2) doped with alkali (Li and Na) and alkaline earth metal (Mg and Ca) supported on MgO. These metal dopants can alter the acid-base property of catalysts, which has an impact on catalysts activity, selectivity and stability. Hence, doped catalysts showed higher C_2 yields than undoped catalysts owing to the presence of strong basic sites (see Figure 4). Among all catalysts, Li-TbO_x/n-MgO showed better activity, C_2 selectivity and C_2 yield at 650 °C. However, undoped catalysts showed higher yield at a lower temperature (<600 °C) than the doped catalysts because the active sites in doped catalysts are blocked with by-product CO_2 at low temperatures.

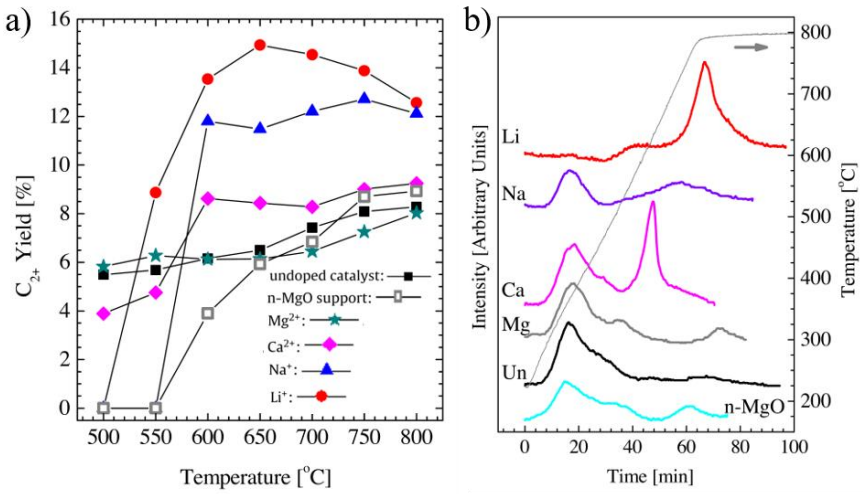

Figure 4. Comparison of C_2 yield in OCM reaction (**a**) with basic strength of the doped and undoped TbOx/n-MgO catalysts (**b**). Redrawn from [38]. Copyright 2018 Elsevier.

Li-doped MgO is one of the best systems for OCM reaction [39–45] because, in this system, an additional electron is produced when each Li^+ cation replaces an Mg^{+2} cation. This excess of an electron is compensated by the formation of electron holes strongly bonded to lattice oxygen, and O^- centers are formed with a strong radical character localized to the O atom, as in the case of Li-doped MgO forming $[Li^+O^-]$ centers. $[Li^+O^-]$ catalyzes the CH_4 dehydrogenation in the following steps:

$$[Li^+O^-] + CH_4 \rightarrow [Li^+OH^-] + CH_3 \quad (1)$$

$$2[Li^+OH^-] \rightarrow [Li^+O^{2-}] + Li^+V + H_2O \quad (2)$$

$$[Li^+O^{2-}] + Li^+V + 1/2O_2 \rightarrow 2[Li^+O^-] \quad (3)$$

Here, 'V' denotes an oxygen vacancy. The [Li^+O^-] centers are generated in Equation (3) again to fulfill a redox cycle [46]. Ali Farsi et al. [41] reported that 7% Li/MgO catalysts were prepared with two different preparation methods, such as incipient wetness impregnation (IWI) and sol-gel (SG). The catalyst prepared by using the sol-gel method exhibited better methane conversion, higher C_2 selectivity, and yield for the desired product than the catalyst prepared by the IWI method. The better performance of the catalyst prepared through the sol-gel method was suggested to relate to the following two factors: (i) it has a significantly larger surface area, and (ii) it comprises a greater quantity of Li incorporated in the MgO matrix. Both of these effects contribute to an increase in the number of active sites in the catalyst. However, at 850 °C, the selectivity of Li/MgO-SG catalyst decreased because of the evaporation of some of the Li from the MgO surface. Qian et al. [42] reported that Li can restructure the MgO surface to expose high-indexed facets such as {110}, {111} and {100} facets; among them, the $Mg_{4c}{}^{2+}$ sites of MgO {110} facets are highly active and selective in catalyzing the OCM reaction, which produces high C_2 selective products by the formation of methyl radical intermediate without other less-stable carbon-containing radicals (CH_2 and CH), which will reduce the methyl radical dissociation and subsequent combustion reaction. Li-doped MgO catalysts with different Li loadings (1.3% and 5.6%) have been prepared by Luo et al. [47]. Different Li contents were observed over both the as-prepared catalysts, but similar Li was present in the used catalysts with different Li surface distribution. Hence, higher CH_4 conversion and C_2 selectivity were observed over Li (5.6%)/MgO than the Li (1.3%)/MgO catalyst because the loss of Li occurred during the reaction process through the movement of these ions from the bulk material to the catalyst surface and successive desorption was responsible for asymmetrical and coarse structures with bare MgO {110} and {111} facets observed in Li (5.6%)/MgO catalysts but not in the Li (1.3%)/MgO. Hence, the main role of Li in MgO-based catalyst during OCM reaction acts as a structural modifier of the active MgO component rather than as an active center. Due to the poor stability of these Li-supported catalysts, some researchers have recently focused on depressing Li-ions' evaporation at high temperatures. Matsumoto et al. [48] proposed that the catalytic activity and selectivity towards desired products were higher over crystalline Li_2CaSiO_4 than Mn-Na_2WO_4/SiO_2, which is considered a state-of-the-art catalyst for OCM. The CH_4 conversion and C_2 selectivity were obtained at 28.3% and 77.5%, respectively, at the temperature of 750 °C for the OCM reaction. In addition, they exhibited higher catalyst durability for 50 h on stream without deactivation and structural changes. The improvement of OCM activity in Li_2CaSiO_4 is likely to result from the combination of multiple cations in the crystal lattice. The structure of Li_2CaSiO_4 consists of a single oxygen site, neighboring with Li, Ca and Si (two Li, two Ca, and one Si atoms). The resulting coordination around oxygen provides a dual character such as strong basicity and lattice stability, which are mainly responsible for CH_4 conversion and C_2 selectivity, respectively. Elkins et al. [49] reported two different types of metal oxide catalysts such as Li-doped TbOx and Sm_2O_3 supported on MgO and they found that the Li-Tb_2O_3/n-MgO catalyst exhibited high activity and selectivity towards desired products at low reaction temperature i.e 650 °C. In addition, the catalyst showed higher stability and lower deactivation rate after 30 h on stream, because the Li addition prompted the reduction of TbO_x phase to Tb_2O_3 and also shifted the Tb 3d core-level electrons to higher binding energy that caused strong Li-TbO_x interactions, which in turn became more active toward C_2 product formation than the SmOx. Table 1 summaries the available data in literature on various Li doped/impregnated catalysts for OCM.

Table 1. OCM reaction over various Li supported/doped catalyst.

Year	Catalyst	Reaction Condition	CH_4 Conv. (%)	C_2 Select. (%)	C_2 Yield (%)	Ref.
1985	7% Li/MgO	CH_4:O_2:N_2 = 1.0: 2.0: 25.0, T = 720 °C flow = 0.83 mL s^{-1}, 4 g catalyst	37.8	50.3	19	[46]
1989	Li(5 wt%)/MgO	CH_4/O_2/He = 78:8:14, T = 675 °C	9.0	82.0	7.4	[50]
2011	7%Li/MgO-IWI	CH_4:O_2:inert = 3:1:3, T = 800 °C, 0.3 g catalyst	26.1	61.3	16	[41]
2011	7%Li/MgO-SG	CH_4:O_2:inert = 3:1:3, T = 800 °C, 0.3 g catalyst	39.6	66.4	26.3	[41]
2014	Li-TbO_x/n-MgO	CH_4:O_2 = 4:1, T = 700 °C, *GHSV = 2400 h^{-1}, 0.4 g catalysts	23.9	63.8	15.3	[49]
2014	Li-Sm_2O_3/n-MgO	CH_4:O_2 = 4:1, T = 700 °C, GHSV = 2400 h^{-1}, 0.4 g catalysts	21.1	62.5	13.2	[49]
2014	1% Li/MgO	CH_4/O_2/N_2 = 4:2:4, T = 800 °C, GHSV = 4500 h^{-1}	38.0	35.0	13.3	[51]
2020	Li_2CaSiO_4	CH_4:O_2:N_2 = 1.0:0.25:8.75, T-800 °C, flow rate = 10 mL/min., 1 g catalyst	30.8	71.8	22.1	[48]
2020	Li_2CaSiO_4	CH_4:O_2:N_2 = 1.0:0.25:8.75, T-800 °C, flow rate = 10 mL/min., 1-g catalyst	45.6	57.7	26.3	[48]
2020	1.3 wt.% Li/MgO	8% CH_4 and 4% O_2 balanced with Ar, T = 750 °C, flow rate: 150 mL/min.	42.0	46.0	19.3	[42]
2020	5.6 wt.% Li/MgO	8% CH_4 and 4% O_2 balanced with Ar, T = 750 °C, flow rate: 150 mL/min.	36	59	21.2	[42]

*GHSV—gas hourly space velocity.

The Li-supported systems, especially Li-MgO catalysts, are among the most studied OCM Catalysts. Because they show a C_2 yield of 20% with higher methane conversion rates at lower temperatures, however, these catalysts suffer from deactivation due to Li vaporization. [Li^+O^-] is specified as the active site for the formation of methyl radical intermediate in OCM reaction, even though many features are still unclear, such as stability of the catalyst, structure activity relationship, and active center; hence, proficient materials are needed to stabilize Li to overcome these issues, and these systems must be stable at high temperatures, where OCM usually occurs. Thus, the synthesis of efficient and Li stable catalysts for OCM is highly challenging. To overcome these issues, in order to improve the catalytic stability of these catalysts, various modifications have been made during the last few decades via the addition of rare-earth oxides or doping with earth alkaline metals or through coordination of multiple ions. As per the previous results, we understand that the mixed-phase oxides have multiple elements with an interface that are believed to show higher activity and stability due to the synergistic effect between the metal oxides. For example, when used Li doped TbO_x and Sm_2O_3 supported on MgO and they found that the Li-Tb_2O_3/n-MgO catalyst exhibited higher stability and lower deactivation rate after 30 h on stream [49], while Li_2CaSiO_4 showed the better catalytic activity and selectivity over Mn-Na_2WO_4/SiO_2 and also exhibited higher catalyst durability for 50 h on stream without deactivation and structural changes for the OCM reaction [48].

2.2. Modified Transition Metal Oxide Catalysts

Mn-$NaWO_4$/SiO_2 catalyst is widely accepted as the most applicable catalyst, with a higher C_2 yield (~27%) in OCM [33,52–60]. Li S-B. et al., J. H. Lunsford et al. and R. M. Lambert et al. groups established Mn-$NaWO_4$/SiO_2 and the optimized chemical composition of this catalyst is 1.9 wt% Mn-5 wt% $NaWO_4$/SiO_2 with Na: W: Mn atom ratio of 2:1:2 [55,61,62]. Ghose et al. [54] prepared different nanostructured complex metal oxides such as Sr–Al complex oxides, La_2O_3, La–Sr–Al complex oxides, and Na_2WO_4-Mn/SiO_2 by using the solution combustion synthesis (SCS) method. Among these catalysts, $Sr_3Al_2O_6$ (double perovskite phase) in the Sr–Al oxides is active for OCM. The La_2O_3 catalyst showed the highest C_2 yields (~13.5%) as compared to similar catalysts presented in the literature. However, the addition of La exhibited a higher C_2 yield even at lower temperatures of 750 °C. The Na_2WO_4-Mn/SiO_2 catalyst was stable and showed a higher C_2 yield (25%) in OCM, which is one of the best results in the literature. Wang et al. [57] carefully explored the effect of Na_2WO_4-Mn/SiO_2 catalysts prepared by different methods such as incipient wetness impregnation (IWI), mixture slurry and the sol-gel method for OCM reaction. As per the different analytical methods, IWI showed that Na, W and Mn are mainly distributed on the catalyst's surface. However, the other two ways are produced more uniform between the surface and bulk on the catalysts. Hence, the mixture slurry method

has excellent stability and is stable during 500 h on stream at 800 °C in the OCM, and during the stream, methane conversion, and C_2 selectivity are maintained at 27–31% and 68–71%, respectively. Yunarti et al. [58] developed promising oxide composite material $Na_2WO_4/Mn/Mg_{0.05}Ti_{0.05}Si_{0.90}O_n$, prepared using a one-pot sol-gel method. This catalyst showed a 23.1% C_2 yield at 800 °C, an 18% higher C_2 selectivity, and a 35% higher C_2 yield than the conventional $Na_2WO_4/Mn/SiO_2$ catalyst, presumably due to Mg and Ti, which are doped in the α-cristobalite SiO_2. These ions can inhibit incorporating Na/W/Mn compounds into the α-cristobalite SiO_2 structure. As a result, Na/W/Mn compounds are exposed to the catalyst's surface, which is more accountable for the higher C_2 selectivity and yield in the OCM reaction. The catalytic results of Mn-$NaWO_4/SiO_2$ indicate synergistic interactions between the various catalyst components (Na, Mn and W), as displayed in Figure 5.

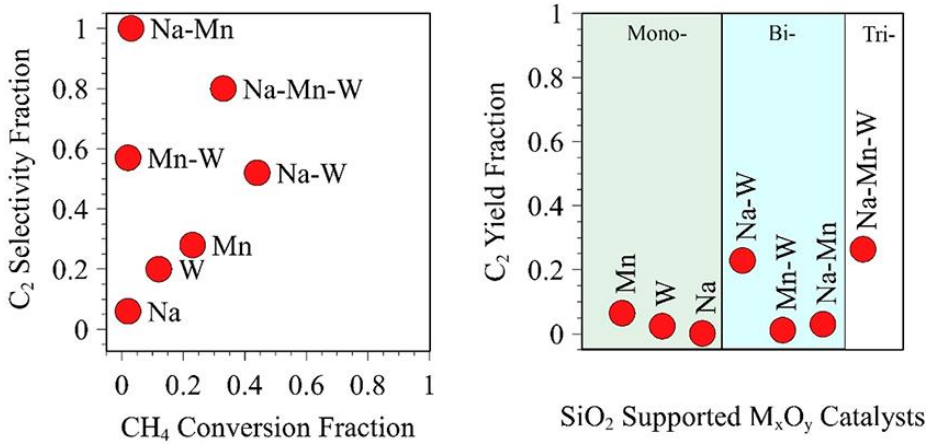

Figure 5. Synergistic effect of SiO_2-based metal oxides to CH_4 conversion and selectivity to 2 (**left**) and C_2 yield (**right**) for OCM reaction. Reproduced with permission from [53]. Copyright 2019 ACS.

If the catalyst contains only Na or W-oxide, it is inactive and unselective. However, catalysts consisting only of Mn-oxide are quite active towards methane combustion. Na and W-oxide catalysts doping enhance their conversion and C_2 selectivity, presumably due to synergy between Na and W components with structural effects and the introduction of surface basic sites. The addition of Na makes it easy to reduce the W-oxide component, which has a positive impact on OCM. Catalysts having both Mn and W oxides showed better C_2 selectivity but were slightly less active. The bi-component system (Na and Mn oxide) is 100% selective but has poor conversion, while, the three-component system (Mn-Na-W oxide supported on SiO_2) shows significantly higher selectivity than bi-component (Na-W, Na-Mn and, and Mn-W) catalysts, although it is slightly less active than the Na-W oxide catalyst. Each component has a specific role in the reaction, and the Na species are generally known to convert SiO_2 support from its primary amorphous phase to crystalline SiO_2 (α-cristobalite) phase, which plays an important role in the OCM reaction and also favors in the migration of Mn and W species to the surface of the catalyst [55,56,63]. The common role of Mn is promoting oxygen mobility between surface-adsorbed and lattice oxygen atoms. The surface Mn sites are responsible for OCM activity and C_2 hydrocarbon selectivity [53]. OCM reaction mechanism for the supported $Mn_2O_3/Na_2WO_4/SiO_2$ catalyst is shown in Figure 6.

Ortiz-Bravo et al. [64] systematically elucidate the electronic and molecular structure of the W and Mn sites on the Mn-Na_2WO_4/SiO_2 catalyst of the corresponding OCM reaction temperature by using different analytical techniques. The Mn-Na_2WO_4/SiO_2 catalyst's structure is highly temperature-dependent; thus, the association of any OCM activity with crystalline phases observed at room temperature is inadequate. In situ TPO-XRD technique clearly displays that the crystalline phases presented at room temperature in the Mn-Na_2WO_4/SiO_2, Na_2WO_4/SiO_2 and WO_3/SiO_2 catalysts are absent at OCM

temperatures (>700 °C). Upon heating in oxidizing conditions, Na and W-oxide's crystalline phases altered to α to β then γ-WO_3; cubic to orthorhombic, then molten Na_2WO_4; and the support SiO_2 phase can be changed α to β-cristobalite. TPO-Raman spectra clearly validate that the bond order of W sites with tetrahedral (T_d) and octahedral (O_h) symmetry varies during the phase transformation. Because all samples retain essentially W^{6+} valence and O_h-Mn^{3+} sites are always present on Mn-Na_2WO_4/SiO_2 catalyst, TPO-XANES spectra expose that bond order differences are due to distortion degree variations. Finally, they established that O_h-W^{6+} sites are inactive in the steady-state OCM tests, but T_d-W^{6+} sites are more active in the presence of O_h-Mn^{3+} sites, which can be helpful for the activation of methane. Table 2 lists the available data in the literature on MnOx-Na_2WO_4/SiO_2 catalysts for OCM.

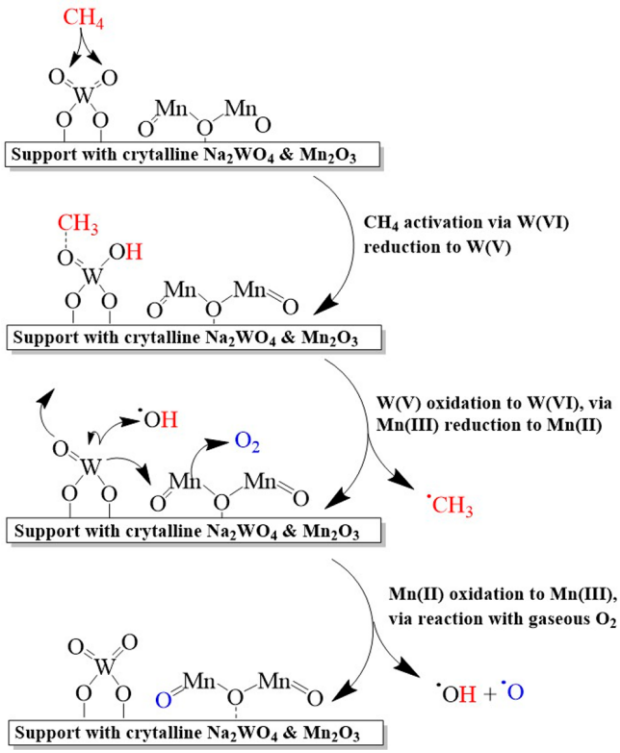

Figure 6. Catalytic OCM mechanism on $Mn_2O_3/Na_2WO_4/SiO_2$. Reproduced with permission from [53]. Copyright 2019 ACS.

Table 2. OCM reaction over various Mn-Na2WO4 supported catalysts.

Year	Catalyst	Reaction Condition	CH_4 Conv. (%)	C_2 Select. (%)	C_2 Yield (%)	Ref.
1989	Na/Mn/MgO	N_2/CH_4/air, P(CH_4) = 0.5 atm; T = 825–925 °C, GHSV = 9600 h^{-1}	11.3−22.4	67−70	-	[63]
1992	5 wt% Mn/1.9 wt.% Na_2WO_4/SiO_2	$CH_4/O_2/N_2$ = 3/1/2.6, T = 800 °C, *WHSV = 36,000 mL g^{-1} h^{-1}	36.8	64.9	23.9	[65]
2013	Na_2WO_4/Mn/SiO_2 (powder)	CH_4/O_2 = 3.5, 60 mol% N_2, T = 850 °C, WHSV = 10,000 h^{-1}	32.0	45.0	14.4	[66]
2013	20%TiO_2/Na_2WO_4/Mn/SiO_2	CH_4/O_2 = 3.5, 60 mol% N_2, T = 850 °C, WHSV = 10,000 h^{-1}	41.0	60.0	24.6	[66]
2014	10% Na_2WO_4–5% Mn/SiO_2	CH_4:O_2 = 32:8, 10% N_2, T = 800 °C, 1 g catalyst	-	-	24.0	[54]
2014	Mn_xO_y–Na_2WO_4/SBA-15	CH_4:O_2:N_2 = 4:1:4, flow—60 mL/min, T = 750 °C, 50 mg catalyst	14.0	70.0	9.8	[60]
2014	Mn_xO_y–Na_2WO_4/SiO_2	CH_4:O_2:N_2 = 4:1:4, flow—60 mL/min, T = 750 °C, 50 mg catalyst	7.0	58.0	4.06	[60]
2015	Mn–Na_2WO_4/n-SiO_2	CH_4:O_2 = 4:1, flow—100 mL with N_2, T-800 °C, 50 mg catalyst	28.5	73.3	18.5	[56]
2015	Mn–Na_2WO_4/n-MgO	CH_4:O_2 = 4:1, flow —100 mL with N_2, T-800 °C, 50 mg catalyst	5.4	64.9	3.2	[56]
2019	MnOx-Na_2WO_4/SiO_2	CH_4:O_2:N_2:Ar = 4:1:1:4, T = 770 °C, GHSV 60,000 cm^3 $h^{-1}g^{-1}$	17.6	70.4	12.4	[67]
2019	MnOx-Na_2WO_4/SiO_2	CH_4:O_2:N_2:Ar = 4:1:1:4, T = 770 °C, GHSV 60,000 cm^3 $h^{-1}g^{-1}$	23.2	70.7	16.4	[67]

*WHSV—Weight hourly space velocity.

Due to their excellent reaction and thermal stability, various supports such as Mg-Ti mixed oxides, SiC, COK-12, SBA-15 were used instead of SiO_2 support to improve the catalyst's performance [60,68–70]. In addition, the promotion of $Mn/Na_2WO_4/SiO_2$ with other metal oxides such as La_2O_3, SnO_2, and CeO_2 have also been conducted in OCM [71–73]. Aimed to optimize the catalytic material for OCM, Sun et al. [74] prepared a series of $Ce_xZr_{1-x}O_2$ catalysts using a sol-gel method with varied Ce/Zr molar ratios and then modified with Mn_2O_3-Na_2WO_4 doping. Among them, $Ce_{0.15}Zr_{0.85}O_2$ containing catalyst exhibited better conversion (25%) and selectivity (67%) even at 660 °C due to generate more O_2^- species, which are responsible for enhanced activity and selectivity at a lower reaction temperature. Moreover, this catalyst showed stable catalytic performance up to 100 h at 660 °C without decreasing the methane conversion (25%) and C_2-C_3 selectivity (67%). Recently, Geo Jong Kim et al. proved that TiO_2 support showed better performance than SiO_2 in Mn/Na_2WO_4-based catalysts. The authors have modified the conventional OCM catalyst (Mn-$NaWO_4/SiO_2$, MNWSi) with TiO_2 (MNWTi) as support and CeO_2 (MNWCeTi) as a promoter. Here they varied the reaction parameters and compared the activities with conventional catalyst. They found that MNWTi catalyst improved methane conversion and C_2 yield. The methane conversion and C_2 yield of this catalyst enhanced from 28.5 to 46.0% and from 12.1 to 25.9% at 775 °C, respectively, as compared to with conventional OCM catalyst, presumably due to having $MnTiO_3$ and Mn_2O_3, with higher Mn species on the surface which are helpful to activate the O_2 at low temperature [75]. Temperatures higher than 700 °C are usually required to initiate this reaction, and higher C_2 yields could be achieved around 800 °C [52,76]. Therefore, catalyst stability and selectivity of hydrocarbons are limited due to the suppression of active sites at very high temperatures and increased non-selective oxidation products. Therefore, there is still a strong motivation to explore novel catalysts with high reaction performance, particularly at low temperatures, to execute this reaction industrially.

2.3. Pyrochlore Catalysts

Pyrochlore ($A_2B_2O_7$) catalysts are promising catalysts for OCM reaction due to their high melting points, thermal stability, tunable M-O bonding, surface alkalinity, and oxygen vacancies [77–82]. The crystal structure of $A_2B_2O_7$ compounds can be tuned with the ionic radius ratio of r_A and r_B sites cations. In detail, pyrochlore structure exists when r_A/r_B is between 1.46 and 1.78, where A and B are distributed in order. The disordered defective fluorite phase formed when r_A/r_B is less than 1.46 and the arrangement of A and B ions are disordered; if r_A/r_B is higher than 1.78, the monoclinic phase will be formed [77,78]. The crystal structure diagram of pyrochlore and defective fluorite can be seen in Figure 7.

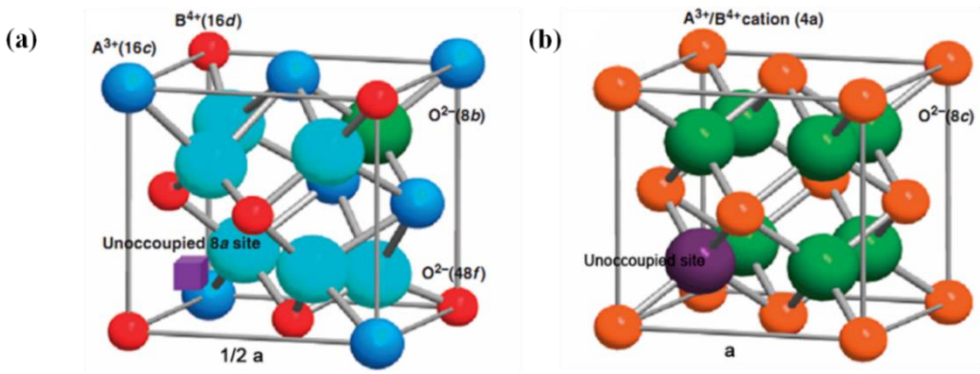

Figure 7. (**a**) Structure of pyrochlore (1/8 unit cell), (**b**) Structure defective fluorite. Reproduced with permission from [83].

The ideal pyrochlore ($A_2B_2O_7$) structure belongs to the space group Fd-3m. It can be written as $A_2B_2O_6$ O′ form, and the formula denotes the existence of two different types of lattice oxygen ions in its crystal structure. Each lattice oxygen ion (O) is coordinated to two A and B sites cations, and the left lattice oxygen ion (O′) is coordinated to four A

sites cation. Compared to the ordered cubic fluorite structure, the pyrochlore compounds contain less of a lattice oxygen ion thus forming inherent oxygen vacancies, which increases the oxygen mobility of the pyrochlore catalysts [80,83,84]. Moreover, a typical pyrochlore ($A_2B_2O_7$) compound containing rare-earth A- and B-site can offer surface alkalinity. In addition, all the characteristics such as thermal stability, surface alkalinity and inherent oxygen vacancies can be altered by replacing or partly substituting of the A and B sites with alkali or alkaline earth metals [85].

Based on these properties, the $A_2B_2O_7$ type of materials has shown some promising catalytic properties in OCM reaction. Petit et al. [81] reported that the catalytic activity of pyrochlore ($A_2B_2O_7$; A—rare earth metal, B—Ti, Sn, Zr) on OCM mainly depended on the B-O bond strength. They found that lower B-O binding energy compounds provided higher C_2 yield. C. A. Mims et al., [86] prepared Bi-Sn pyrochlore catalysts and then expanded the series of $Bi_2Sn_{2-x}Bi_xO_{7-x/2}$ ($0 \leq x \leq 0.86$) with substitution of Bi cation in the B site of the pyrochlore. These catalysts were used for OCM and have shown improvement in C_2 selectivity as the number of Bi cations at B sites increased. In addition, A. C. Roger et al. [87] synthesized Sn-deficient pyrochlore ($Sm_2Sn_2O_7$) catalysts by using a sol-gel method, and these catalysts improved the C_2 yield in the OCM reaction.

Recently, Wang and co-workers have developed different types of pyrochlore catalysts and examined their properties', such as r_A/r_B ratios, effect on crystalline structures, surface active oxygen sites, intrinsic oxygen vacancies and surface alkaline sites, being essential for OCM reaction [77,78,85]. A series of $Ln_2Ce_2O_7$ (Ln = La, Pr, Sm and Y) catalysts have been developed and demonstrated as the defective cubic fluorite phase. Among them, $La_2Ce_2O_7$ exhibited the highest C_2 yield of 16.6% at 750 °C due to the moderated alkaline sites and surface active oxygen species [77]. To examine the relationship between phase structure and reactivity of pyrochlore catalysts for the OCM, three model $La_2B_2O_7$ (B-Ti, Zr and Ce) pyrochlore compounds with different crystal phases have been prepared. The crystalline phase of $La_2B_2O_7$ differs from monoclinic layered perovskite ($La_2Ti_2O_7$) to ordered cubic pyrochlore ($La_2Zr_2O_7$) and defective cubic fluorite ($La_2Ce_2O_7$) by declining the r_A/r_B ratios. These catalytic activities and C_2 yields follow the order of $La_2Ce_2O_7$ > $La_2Zr_2O_7$ > $La_2Ti_2O_7$, being consistent with higher surface active oxygen species and moderate surface alkaline sites [78]. Aimed to optimize the $La_2Ce_2O_7$ catalytic material for OCM, a series of catalysts were fabricated by a sol-gel method with varied La/Ce molar ratios and being doped with Ca, which had a close ionic radius with La and Ce ions. Among them, $La_2Ce_{1.5}Ca_{0.5}O_7$ showed better yields (22.5%) at 750 °C due to its enhanced surface alkalinity and oxygen mobility with doping of Ca additive [85]. Table 3 lists the available data in the literature on pyrochlore catalysts for OCM.

Table 3. OCM reaction over various pyrochlore catalysts.

Year	Catalyst	Reaction Condition	CH_4 Conv. (%)	C_2 Select. (%)	C_2 Yield (%)	Ref.
1989	$La_2Sn_2O_7$	CH_4:O_2 = 2:1 and flow rate = 27 mL/min., T = 727 °C	29.7	15	4.4	[88]
1989	$Dy_2Sn_2O_7$	CH_4:O_2 = 2:1 and flow rate = 27 mL/min., T = 727 °C	30.4	21.9	6.6	[88]
1992	$Sm_2Sn_2O_7$	CH_4/O_2 = 2, T = 750 °C, 67 mg catalyst, flow = 4.51 g h^{-1}	40.4	48.8	19.7	[81]
1992	$Sm_2Zr_2O_7$	CH_4/O_2 = 2, T = 750 °C, 67 mg catalyst, flow = 4.51 g h^{-1}	28.4	10	2.8	[81]
1992	$Sm_2Ti_2O_7$	CH_4/O_2 = 2, T = 750 °C, 67 mg catalyst, flow = 4.51 g h^{-1}	31.9	22.1	7.04	[81]
2018	$La_2Ce_2O_7$	CH_4/O_2 = 4:1, T = 800 °C, WHSV = 18,000 mL h^{-1} g^{-1}	28.3	58.5	16.6	[77]
2018	$Pr_2Ce_2O_7$	CH_4/O_2 = 4:1, T = 800 °C, WHSV = 18,000 mL h^{-1} g^{-1}	15	32.6	4.9	[77]
2018	$Sm_2Ce_2O_7$	CH_4/O_2 = 4:1, T = 800 °C, WHSV = 18,000 mL h^{-1} g^{-1}	22.6	51	11.5	[77]
2018	$Y_2Ce_2O_7$	CH_4/O_2 = 4:1, T = 800 °C, WHSV = 18,000 mL h^{-1} g^{-1}	23.3	52.4	12.2	[77]
2019	$La_2Zr_2O_7$	CH_4:O_2:N_2 = 4:1:5, T = 800 °C, WHSV = 18,000 mL h^{-1} g^{-1}	24.2	50.4	12.2	[78]
2019	$La_2Ti_2O_7$	CH_4:O_2:N_2 = 4:1:5, T = 800 °C, WHSV = 18,000 mL h^{-1} g^{-1}	18	32.3	5.8	[78]
2019	$La_2Ce_{1.5}Ca_{0.5}O_7$	CH_4:O_2:N_2 = 4:1:5, T = 800 °C, WHSV = 18,000 mL h^{-1} g^{-1}	32	70	22.4	[85]
2019	$La_{1.5}Ca_{0.5}Ce_2O_7$	CH_4:O_2:N_2 = 4:1:5, T = 800 °C, WHSV = 18,000 mL h^{-1} g^{-1}	28	47	13.2	[85]

$La_2Ce_2O_7$ pyrochlore catalysts have been synthesized in our group using the sol-gel method and further doped with Sr through optimization on Sr loading [89]. The defective cubic fluorite phase remained after Sr doping. Introduction of Sr in $La_2Ce_2O_7$, especially allowing strontium to enter into the crystal lattice ($La_{1.5}Sr_{0.5}Ce_2O_7$), significantly improved the mobility of lattice oxygen compared to the undoped pyrochlore ($La_2Ce_2O_7$)

and impregnated Sr sample (8% Sr/$La_2Ce_2O_7$) (Figure 8). The relative contents of O^{2-} lattice oxygen of the three prepared catalysts, i.e., doped, impregnated and undoped, followed the order of $La_{1.5}Sr_{0.5}Ce_2O_7$ > 8% Sr/$La_2Ce_2O_7$ > $La_2Ce_2O_7$ as shown in XPS results (see Figure 9, Table 4); these obtained results were in line with H_2-TPR results and the OCM reaction performance. A sample containing a large amount of lattice oxygen sites showed better reaction performance (see Figure 11). CO_2-TPD results (see Figure 10, Table 5) revealed that introduction of Sr enhanced the ratio of strong basic sites, which is usually considered as a beneficial factor for producing C_2 products. As a result, the selectivity and yield of C_2-based products could reach 57% and 14%, respectively, over $La_{1.5}Sr_{0.5}Ce_2O_7$ catalysts at 800 °C (see Figure 11). Moreover, this catalyst showed stable catalytic performance up to 30 h without deactivation (see Figure 12).

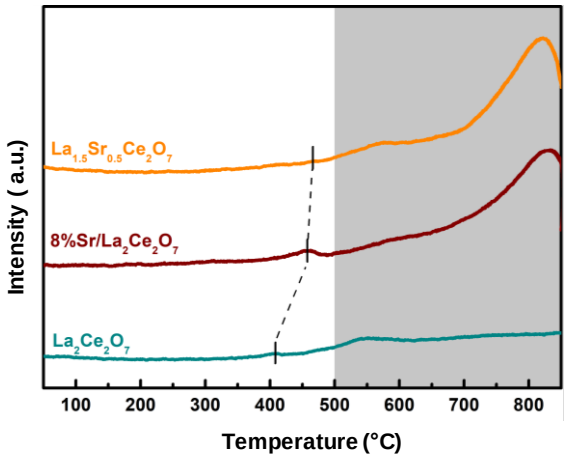

Figure 8. H_2-TPR profile of the indicated catalysts [89].

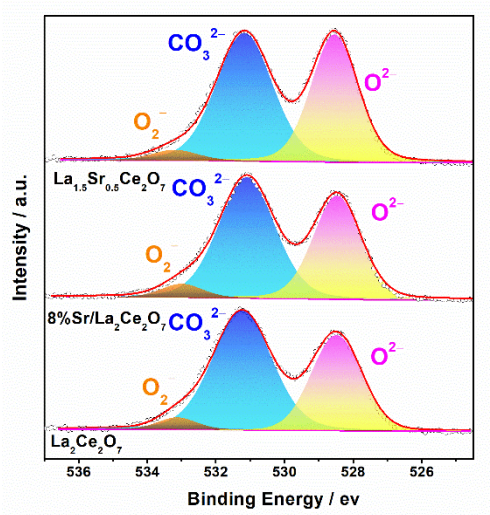

Figure 9. XPS O 1s spectra of the indicated catalysts [89].

Table 4. H_2-TPR and XPS results of the catalysts [89].

Catalysts	Hydrogen Consumption/(mL·g^{-1})		R1/%	R2/%	O 1s/eV			R3/%
	>500 °C	Total			O^{2-}	CO_3^{2-}	O_2^-	
$La_2Ce_2O_7$	6.31	7.76	3.3	81.4	528.5	531.2	533.1	37.4
8% Sr/$La_2Ce_2O_7$	14.82	16.77	7.1	88.4	528.5	531.1	533.0	40.2
$La_{1.5}Sr_{0.5}Ce_2O_7$	18.11	20.10	8.3	90.1	528.6	531.2	533.2	43.6

R1 refers to the percentage of actual hydrogen consumption to theoretical hydrogen consumption (calculated by the stoichiometric ratio). R2 refers to the percentage of hydrogen consumption above 500 °C to the total hydrogen consumption. R3 refers to the relative ratio of $O^{2-}/(O^{2-} + CO_3^{2-} + O_2^-)$.

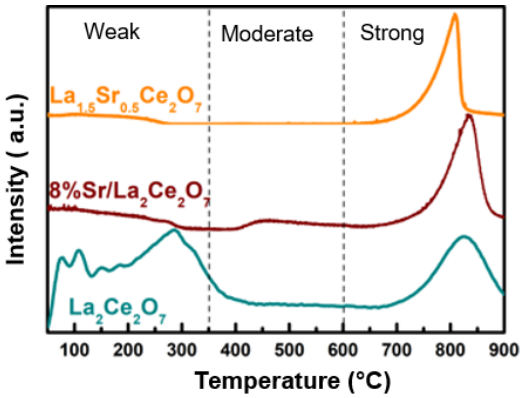

Figure 10. CO_2-TPD profile of the indicated catalysts [89].

Table 5. CO_2-TPD quantification results of the catalysts [89].

Catalysts	CO_2 Desorption Ratio/%		
	50–350 °C	350–600 °C	600–900 °C
$La_2Ce_2O_7$	47.8	18.2	34.0
8% Sr/$La_2Ce_2O_7$	27.0	8.3	64.7
$La_{1.5}Sr_{0.5}Ce_2O_7$	20.8	0.9	78.3

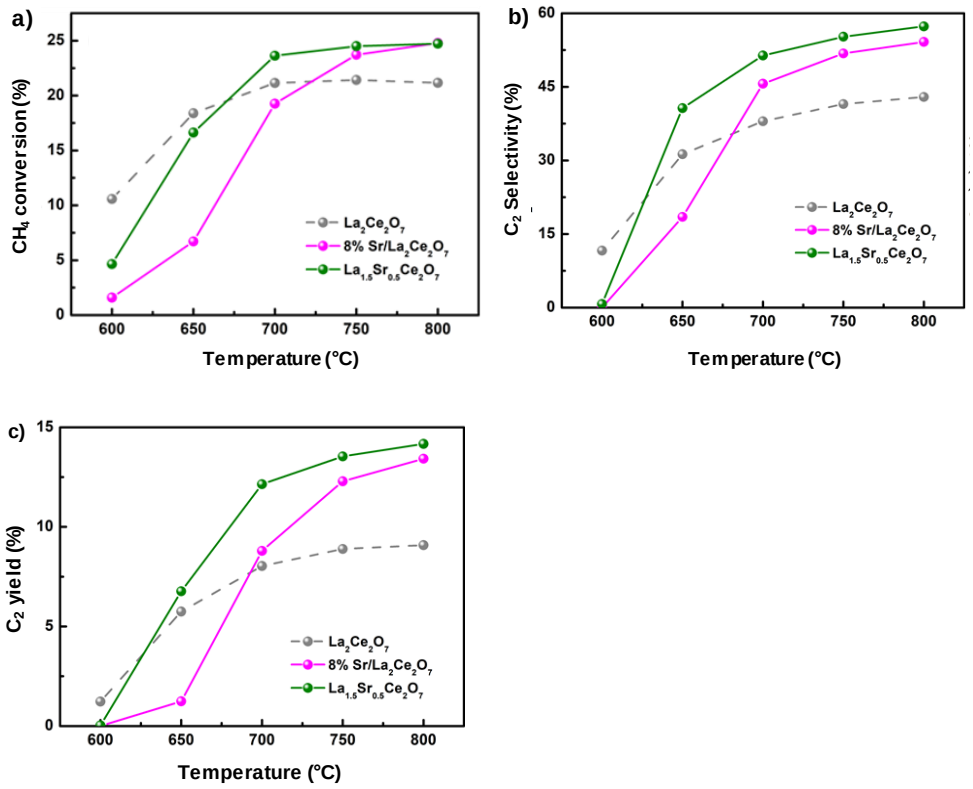

Figure 11. OCM reaction over the indicated catalysts: (**a**) CH_4 conversion, (**b**) C_2 selectivity, (**c**) C_2 yield. Reaction condition: CH_4:O_2:N_2 = 4:1:5, WHSV = 72,000 mL·g^{-1}·h^{-1} [89].

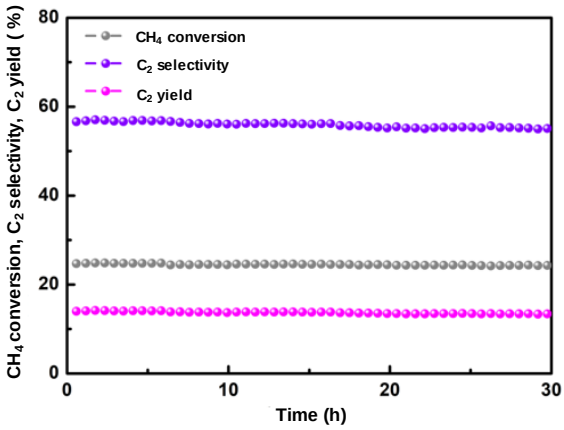

Figure 12. Stability test at 800 °C with the $La_{1.5}Sr_{0.5}Ce_2O_7$ catalyst. Reaction condition: CH_4:O_2:N_2 = 4:1:5, WHSV = 72,000 mL·g^{-1}·h^{-1} [89].

In another study, we substitute the B site of $La_2Ce_2O_7$ by Ca^{2+} (0.1 nm) and Sr^{2+} (0.126 nm), respectively, which have an identical atomic radius to Ce^{4+} (0.097 nm). These catalysts showed better selectivity and yield than host compounds. XRD results (Figure 13) reveal that all doped samples presented well-resolved peaks analogous to their host pyrochlore materials with only a slight shift of the 2θ values, signifying those doped compounds have similar phase structures to their host compounds. The quantitative analysis of H_2-TPR results (see Figure 14, Table 6) revealed that the reduction temperature and reducible lattice oxygen species of doped samples were significantly enhanced than the un-doped sample; consequently, this rise in the reduction temperature indicated higher M-O bonding strength. Among these doped catalysts, $La_2Ce_{1.5}Sr_{0.5}O_7$ showed a higher reduction temperature and contained a larger amount of lattice oxygen, which was primarily responsible for the higher C_2 selectivity in the OCM reaction. Therefore, this catalyst exhibited better yield at 800 °C (see Figure 15).

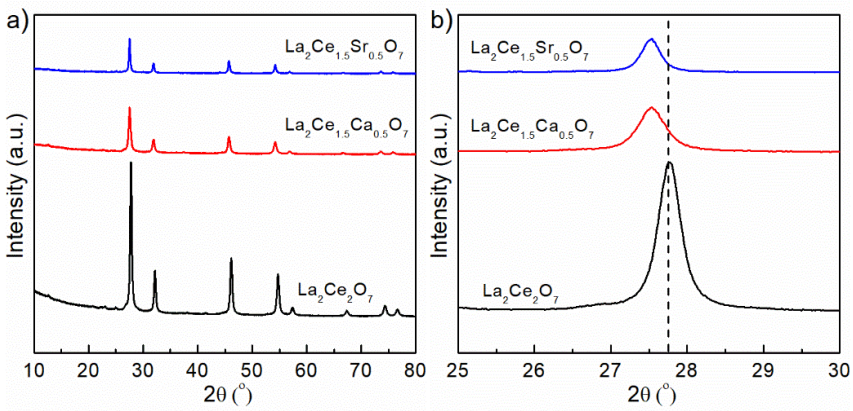

Figure 13. (**a**) XRD patterns of the indicated catalysts, (**b**) enlarge images of the main reflection in figure-a.

Table 6. H_2-TPR results of the catalysts.

Catalysts	Hydrogen Consumption/(mL·g^{-1}) >500 °C	Hydrogen Consumption/(mL·g^{-1}) Total	R1/%
$La_2Ce_2O_7$	6.31	7.76	81.4
$La_2Ce_{1.5}Ca_{0.5}O_7$	10.55	11.43	92.30
$La_2Ce_{1.5}Sr_{0.5}O_7$	11.99	12.64	94.85

R1 refers to the percentage of hydrogen consumption above 500 °C to the total hydrogen consumption.

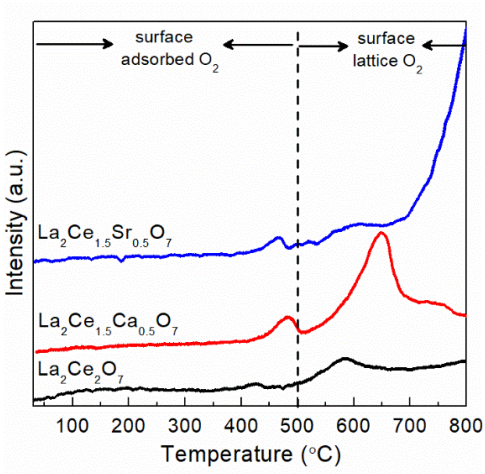

Figure 14. H_2-TPR profile of the indicated catalysts.

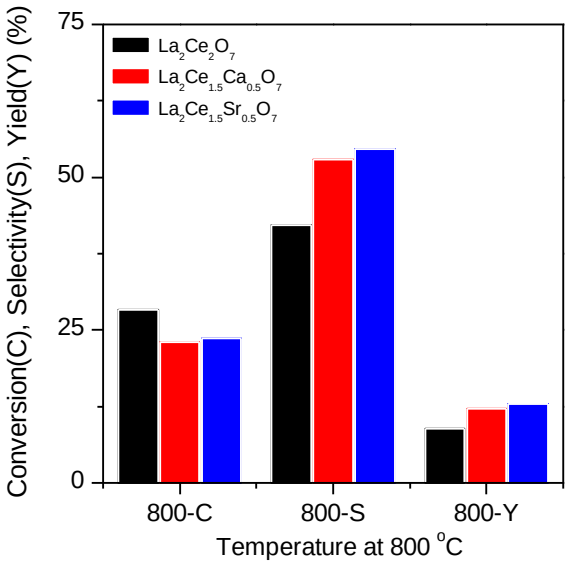

Figure 15. OCM reaction over the $La_2Ce_2O_7$ and B site substitution catalysts at 800 °C. Reaction condition: CH_4:O_2:N_2 = 4:1:5, WHSV = 72,000 mL·g^{-1}·h^{-1}.

3. Conclusions and Perspective

Natural gas has attracted considerable attention because of fluctuating fuel prices around the world and continuous depletion of energy reserves of crude oil, and also due to its unique features such as a clean source of fossil energy and as a feedstock of various other chemicals including ethylene. Methane is a major component of natural gas, and its deposits are expected to be higher than crude oil in the coming future. Ethylene is considered as a key building block in the field of industrial chemical production. Therefore, a strong economic interest is developing in the processes that allow the conversion of methane to high value-added products such as numerous intermediate products such as polymers, i.e., polyethylene, polystyrene; and hydrocarbons i.e., ethylene. In this regard, oxidative coupling methane (OCM) is an important reaction process for the catalytic upgrading of methane in natural gas and/or shale gas to ethylene for meeting its industrial production demand. This review article mainly consolidated recent literature that captured and evaluated the modifications during the catalyst development progress made regarding the OCM reaction.

The development of commercially viable catalysts for OCM reaction is still a crucial challenge for researchers. In order to obtain the desired goal, recently, various catalysts have been used based on the metal oxides such as reducible metal oxides, rare earth oxides,

alkaline earth oxides, alkali-promoted metal oxides or mixed oxides, and pyrochlore compounds individually or in various combinations. In the current review, we have explored a variety of catalysts such as alkali/alkaline earth metals-based catalysts viz., Li supported catalysts, Mn-$NaWO_4/SiO_2$ and pyrochlore catalysts. It has been reviewed that catalyst performance depends on several factors such as their preparation method, structural composition and the basicity of catalyst. From the reports, we have understood that active sites, facile oxygen abundance, surface alkalinity and metal-support interactions are crucial for catalytic performance. However, by using these catalysts, a low yield of C_2 products still was achieved (<30%) and could not match the commercial requirement.

4. Perspective

Li-based catalysts have shown higher activity and selectivity in OCM reaction due to strong basicity and M-O bond. However, the catalysts suffer deactivation during the reaction, being related to the loss of Li at high operation temperatures. Therefore, how to stabilize Li and restrain its evaporation at high temperatures by forming strong metal support interactions might be a possible solution for this. Meanwhile, it is noted that pyrochlore ($A_2B_2O_7$) catalysts have shown some promising properties for OCM reaction due to high melting points, thermal stability, tunable M-O bonding and moderate surface alkalinity. Using pyrochlore as the stable support to load Li might generate strong interactions between Li and pyrochlore, forming new phases of Li compounds, such as Li_2SnO_3 and $LiLaO_2$, which provides a feasible way to stabilize Li. Some preliminary results have been obtained in our group to show its promising perspectives. In addition, optimization of experimental conditions for the synthesis of pyrochlore catalysts, especially for those with specific morphology, might improve the catalytic performance at lower temperatures. Discrimination of the key factors caused by A/B regulation or substitution and their interactions with the doped Li give the opportunity to further enhance the catalytic activity and selectivity as well as the stability by stabilizing Li with optimized pyrochlore.

Author Contributions: Conceptualization, Methodology, Investigation, Writing Review & Editing, Visualization, P.R.M.; Investigation, Methodology, Review & Editing, Visualization, Y.L.; Reviewing and Editing, G.W.; Reviewing and Editing; Y.D.; Conceptualization, Supervision, Writing—Reviewing and Editing, Funding acquisition, C.S. All authors have read and agreed to the published version of the manuscript.

Funding: The work was supported by the National Natural Science Foundation of China (Nos. 21872014, 21932002 and 21902018), the National Key R&D Program of China (No. 2017YFA0700103), the Liaoning Revitalization Talent Program (XLYC2008032) and the Fundamental Research Funds for the Central Universities (DUT20ZD205).

Conflicts of Interest: The authors declare no conflict of interests.

References

1. Sattler, J.J.H.B.; Ruiz-Martinez, J.; Santillan-Jimenez, E.; Weckhuysen, B.M. Catalytic dehydrogenation of light alkanes on metals and metal oxides. *Chem. Rev.* **2014**, *114*, 10613–10653. [CrossRef] [PubMed]
2. Wood, D.A.; Nwaoha, C.; Towler, B.F. Gas-to-liquids (GTL): A review of an industry offering several routes for monetizing natural gas. *J. Nat. Gas Sci. Eng.* **2012**, *9*, 196–208. [CrossRef]
3. Galadima, A.; Muraza, O. Revisiting the oxidative coupling of methane to ethylene in the golden period of shale gas: A review. *J. Ind. Eng. Chem.* **2016**, *37*, 1–13. [CrossRef]
4. Guo, B.; Shan, J.; Feng, Y. Productivity of blast-fractured wells in liquid-rich shale gas formations. *J. Nat. Gas Sci. Eng.* **2014**, *18*, 360–367. [CrossRef]
5. Seifzadeh Haghighi, S.; Rahimpour, M.R.; Raeissi, S.; Dehghani, O. Investigation of ethylene production in naphtha thermal cracking plant in presence of steam and carbon dioxide. *Chem. Eng. J.* **2013**, *228*, 1158–1167. [CrossRef]
6. Le Van Mao, R.; Yan, H.; Muntasar, A.; Al-Yassir, N. Chapter 7—Blending of non-petroleum compounds with current hydrocarbon feeds to use in the thermo-catalytic steam-cracking process for the selective production of light olefins. In *New and Future Developments in Catalysis*; Suib, S.L., Ed.; Elsevier: Amsterdam, The Netherlands, 2013; pp. 143–173.
7. Keyvanloo, K.; Towfighi, J.; Sadrameli, S.M.; Mohamadalizadeh, A. Investigating the effect of key factors, their interactions and optimization of naphtha steam cracking by statistical design of experiments. *J. Anal. Appl. Pyrolysis* **2010**, *87*, 224–230. [CrossRef]

8. Corma, A.; Mengual, J.; Miguel, P.J. IM-5 zeolite for steam catalytic cracking of naphtha to produce propene and ethene. An alternative to ZSM-5 zeolite. *Appl. Catal. A Gen.* **2013**, *460–461*, 106–115. [CrossRef]
9. Dry, M.E. The Fischer–Tropsch process: 1950–2000. *Catal. Today* **2002**, *71*, 227–241. [CrossRef]
10. Schulz, H. Short history and present trends of Fischer–Tropsch synthesis. *Appl. Catal. A Gen.* **1999**, *186*, 3–12. [CrossRef]
11. Tian, P.; Wei, Y.; Ye, M.; Liu, Z. Methanol to olefins (MTO): From fundamentals to commercialization. *ACS Catal.* **2015**, *5*, 1922–1938. [CrossRef]
12. Olsbye, U.; Svelle, S.; Bjørgen, M.; Beato, P.; Janssens, T.V.W.; Joensen, F.; Bordiga, S.; Lillerud, K.P. Conversion of methanol to hydrocarbons: How zeolite cavity and pore size controls product selectivity. *Angew. Chem. Int. Ed.* **2012**, *51*, 5810–5831. [CrossRef]
13. Guo, X.; Fang, G.; Li, G.; Ma, H.; Fan, H.; Yu, L.; Ma, C.; Wu, X.; Deng, D.; Wei, M.; et al. Direct, nonoxidative conversion of methane to ethylene, aromatics, and hydrogen. *Science* **2014**, *344*, 616–619. [CrossRef] [PubMed]
14. Zhao, M.; Ke, S.; Wu, H.; Xia, W.; Wan, H. Flower-like Sr-La_2O_3 microspheres with hierarchically porous structures for oxidative coupling of methane. *Ind. Eng. Chem. Res.* **2019**, *58*, 22847–22856. [CrossRef]
15. Lopes, L.B.; Vieira, L.H.; Assaf, J.M.; Assaf, E.M. Effect of Mg substitution on $LaTi_{1-x}Mg_xO_{3+\delta}$ catalysts for improving the C_2 selectivity of the oxidative coupling of methane. *Catal. Sci. Technol.* **2021**, *11*, 283–296. [CrossRef]
16. Sato, A.; Ogo, S.; Kamata, K.; Takeno, Y.; Yabe, T.; Yamamoto, T.; Matsumura, S.; Hara, M.; Sekine, Y. Ambient-temperature oxidative coupling of methane in an electric field by a cerium phosphate nanorod catalyst. *Chem. Commun.* **2019**, *55*, 4019–4022. [CrossRef] [PubMed]
17. Schmack, R.; Friedrich, A.; Kondratenko, E.V.; Polte, J.; Werwatz, A.; Kraehnert, R. A meta-analysis of catalytic literature data reveals property-performance correlations for the OCM reaction. *Nat. Commun.* **2019**, *10*, 441. [CrossRef]
18. Pirro, L.; Mendes, P.S.F.; Kemseke, B.; Vandegehuchte, B.D.; Marin, G.B.; Thybaut, J.W. From catalyst to process: Bridging the scales in modeling the OCM reaction. *Catal. Today* **2021**, *365*, 35–45. [CrossRef]
19. Gambo, Y.; Jalil, A.A.; Triwahyono, S.; Abdulrasheed, A.A. Recent advances and future prospect in catalysts for oxidative coupling of methane to ethylene: A review. *J. Ind. Eng. Chem.* **2018**, *59*, 218–229. [CrossRef]
20. Grant, J.T.; Venegas, J.M.; McDermott, W.P.; Hermans, I. Aerobic Oxidations of Light Alkanes over Solid Metal Oxide Catalysts. *Chem. Rev.* **2018**, *118*, 2769–2815. [CrossRef]
21. Lomonosov, V.I.; Sinev, M.Y. Oxidative coupling of methane: Mechanism and kinetics. *Kinet. Catal.* **2016**, *57*, 647–676. [CrossRef]
22. Keller, G.E.; Bhasin, M.M. Synthesis of ethylene via oxidative coupling of methane: I. Determination of active catalysts. *J. Catal.* **1982**, *73*, 9–19. [CrossRef]
23. Ito, T.; Lunsford, J.H. Synthesis of ethylene and ethane by partial oxidation of methane over lithium-doped magnesium oxide. *Nature* **1985**, *314*, 721–722. [CrossRef]
24. Jiang, T.; Song, J.; Huo, M.; Yang, N.; Liu, J.; Zhang, J.; Sun, Y.; Zhu, Y. La_2O_3 catalysts with diverse spatial dimensionality for oxidative coupling of methane to produce ethylene and ethane. *RSC Adv.* **2016**, *6*, 34872–34876. [CrossRef]
25. Papa, F.; Luminita, P.; Osiceanu, P.; Birjega, R.; Akane, M.; Balint, I. Acid–base properties of the active sites responsible for C_{2+} and CO_2 formation over MO–Sm_2O_3 (M = Zn, Mg, Ca and Sr) mixed oxides in OCM reaction. *J. Mol. Catal. A Chem.* **2011**, *346*, 46–54. [CrossRef]
26. Wang, P.; Zhao, G.; Wang, Y.; Lu, Y. $MnTiO_3$-driven low-temperature oxidative coupling of methane over TiO_2-doped Mn_2O_3-Na_2WO_4/SiO_2 catalyst. *Sci. Adv.* **2017**, *3*, e1603180. [CrossRef]
27. Bai, L.; Polo-Garzon, F.; Bao, Z.; Luo, S.; Moskowitz, B.M.; Tian, H.; Wu, Z. Impact of Surface Composition of $SrTiO_3$ Catalysts for Oxidative Coupling of Methane. *ChemCatChem* **2019**, *11*, 2107–2117. [CrossRef]
28. Lee, J.S.; Oyama, S.T. Oxidative Coupling of Methane to Higher Hydrocarbons. *Catal. Rev.* **1988**, *30*, 249–280. [CrossRef]
29. Zavyalova, U.; Holena, M.; Schlögl, R.; Baerns, M. Statistical analysis of past catalytic data on oxidative methane coupling for new insights into the composition of high-performance catalysts. *ChemCatChem* **2011**, *3*, 1935–1947. [CrossRef]
30. Horn, R.; Schlögl, R. Methane activation by heterogeneous catalysis. *Catal. Lett.* **2015**, *145*, 23–39. [CrossRef]
31. Voskresenskaya, E.N.; Roguleva, V.G.; Anshits, A.G. Oxidant activation over structural defects of oxide catalysts in oxidative methane coupling. *Catal. Rev.* **1995**, *37*, 101–143. [CrossRef]
32. Ferreira, V.J.; Tavares, P.; Figueiredo, J.L.; Faria, J.L. Effect of Mg, Ca, and Sr on CeO_2 based catalysts for the oxidative coupling of methane: Investigation on the oxygen species responsible for catalytic performance. *Ind. Eng. Chem. Res.* **2012**, *51*, 10535–10541. [CrossRef]
33. Yıldız, M. Mesoporous TiO_2-rutile supported MnxOy-Na_2WO_4: Preparation, characterization and catalytic performance in the oxidative coupling of methane. *J. Ind. Eng. Chem.* **2019**, *76*, 488–499. [CrossRef]
34. Ivanov, D.V.; Isupova, L.A.; Gerasimov, E.Y.; Dovlitova, L.S.; Glazneva, T.S.; Prosvirin, I.P. Oxidative methane coupling over Mg, Al, Ca, Ba, Pb-promoted $SrTiO_3$ and Sr_2TiO_4: Influence of surface composition and microstructure. *Appl. Catal. A Gen.* **2014**, *485*, 10–19. [CrossRef]
35. Peng, L.; Xu, J.; Fang, X.; Liu, W.; Xu, X.; Liu, L.; Li, Z.; Peng, H.; Zheng, R.; Wang, X. SnO_2 based catalysts with low-temperature performance for oxidative coupling of methane: Insight into the promotional effects of alkali-metal oxides. *Eur. J. Inorg. Chem.* **2018**, *2018*, 1787–1799. [CrossRef]
36. Cong, L.; Zhao, Y.; Li, S.; Sun, Y. Sr-doping effects on La_2O_3 catalyst for oxidative coupling of methane. *Chin. J. Catal.* **2017**, *38*, 899–907. [CrossRef]

37. Kim, I.; Lee, G.; Na, H.B.; Ha, J.-M.; Jung, J.C. Selective oxygen species for the oxidative coupling of methane. *Mol. Catal.* **2017**, *435*, 13–23. [CrossRef]
38. Elkins, T.W.; Roberts, S.J.; Hagelin-Weaver, H.E. Effects of alkali and alkaline-earth metal dopants on magnesium oxide supported rare-earth oxide catalysts in the oxidative coupling of methane. *Appl. Catal. A Gen.* **2016**, *528*, 175–190. [CrossRef]
39. Senanayake, S.D.; Rodriguez, J.A.; Weaver, J.F. Low temperature activation of methane on metal-oxides and complex interfaces: Insights from surface science. *Acc. Chem. Res.* **2020**, *53*, 1488–1497. [CrossRef]
40. Schröder, D.; Roithová, J. Low-temperature activation of methane: It also works without a transition metal. *Angew. Chem. Int. Ed.* **2006**, *45*, 5705–5708. [CrossRef]
41. Farsi, A.; Moradi, A.; Ghader, S.; Shadravan, V. Oxidative coupling of methane over Li/MgO: Catalyst and nanocatalyst performance. *Chin. J. Chem. Phys.* **2011**, *24*, 70–76. [CrossRef]
42. Qian, K.; You, R.; Guan, Y.; Wen, W.; Tian, Y.; Pan, Y.; Huang, W. Single-Site catalysis of Li-MgO catalysts for oxidative coupling of methane reaction. *ACS Catal.* **2020**, *10*, 15142–15148. [CrossRef]
43. Kwapien, K.; Paier, J.; Sauer, J.; Geske, M.; Zavyalova, U.; Horn, R.; Schwach, P.; Trunschke, A.; Schlögl, R. Sites for methane activation on lithium-doped magnesium oxide surfaces. *Angew. Chem. Int. Ed.* **2014**, *53*, 8774–8778. [CrossRef]
44. Schwach, P.; Frandsen, W.; Willinger, M.-G.; Schlögl, R.; Trunschke, A. Structure sensitivity of the oxidative activation of methane over MgO model catalysts: I. Kinetic study. *J. Catal.* **2015**, *329*, 560–573. [CrossRef]
45. Berger, T.; Schuh, J.; Sterrer, M.; Diwald, O.; Knözinger, E. Lithium ion induced surface reactivity changes on MgO nanoparticles. *J. Catal.* **2007**, *247*, 61–67. [CrossRef]
46. Ito, T.; Wang, J.; Lin, C.H.; Lunsford, J.H. Oxidative dimerization of methane over a lithium-promoted magnesium oxide catalyst. *J. Am. Chem. Soc.* **1985**, *107*, 5062–5068. [CrossRef]
47. Luo, L.; Jin, Y.; Pan, H.; Zheng, X.; Wu, L.; You, R.; Huang, W. Distribution and role of Li in Li-doped MgO catalysts for oxidative coupling of methane. *J. Catal.* **2017**, *346*, 57–61. [CrossRef]
48. Matsumoto, T.; Saito, M.; Ishikawa, S.; Fujii, K.; Yashima, M.; Ueda, W.; Motohashi, T. High catalytic activity of crystalline lithium calcium silicate for oxidative coupling of methane originated from crystallographic joint effects of multiple cations. *ChemCatChem* **2020**, *12*, 1968–1972. [CrossRef]
49. Elkins, T.W.; Neumann, B.; Bäumer, M.; Hagelin-Weaver, H.E. Effects of Li Doping on MgO-Supported Sm_2O_3 and TbOx Catalysts in the Oxidative Coupling of Methane. *ACS Catal.* **2014**, *4*, 1972–1990. [CrossRef]
50. Lunsford, J.H. The Catalytic oxidative coupling of methane. *Angew. Chem. Int. Ed.* **1995**, *34*, 970–980. [CrossRef]
51. Raouf, F.; Taghizadeh, M.; Yousefi, M. Influence of CaO–ZnO supplementation as a secondary catalytic bed on the oxidative coupling of methane. *React. Kinet. Mech. Catal.* **2014**, *112*, 227–240. [CrossRef]
52. Arndt, S.; Otremba, T.; Simon, U.; Yildiz, M.; Schubert, H.; Schomäcker, R. Mn–Na_2WO_4/SiO_2 as catalyst for the oxidative coupling of methane. What is really known? *Appl. Catal. A Gen.* **2012**, *425–426*, 53–61. [CrossRef]
53. Kiani, D.; Sourav, S.; Baltrusaitis, J.; Wachs, I.E. Oxidative Coupling of methane (OCM) by SiO_2-supported tungsten oxide catalysts promoted with Mn and Na. *ACS Catal.* **2019**, *9*, 5912–5928. [CrossRef]
54. Ghose, R.; Hwang, H.T.; Varma, A. Oxidative coupling of methane using catalysts synthesized by solution combustion method: Catalyst optimization and kinetic studies. *Appl. Catal. A Gen.* **2014**, *472*, 39–46. [CrossRef]
55. Palermo, A.; Holgado Vazquez, J.P.; Lee, A.F.; Tikhov, M.S.; Lambert, R.M. Critical influence of the amorphous silica-to-cristobalite phase transition on the performance of $Mn/Na_2WO_4/SiO_2$ catalysts for the oxidative coupling of methane. *J. Catal.* **1998**, *177*, 259–266. [CrossRef]
56. Elkins, T.W.; Hagelin-Weaver, H.E. Characterization of Mn–Na_2WO_4/SiO_2 and Mn–Na_2WO_4/MgO catalysts for the oxidative coupling of methane. *Appl. Catal. A Gen.* **2015**, *497*, 96–106. [CrossRef]
57. Wang, J.; Chou, L.; Zhang, B.; Song, H.; Zhao, J.; Yang, J.; Li, S. Comparative study on oxidation of methane to ethane and ethylene over Na_2WO_4–Mn/SiO_2 catalysts prepared by different methods. *J. Mol. Catal. A Chem.* **2006**, *245*, 272–277. [CrossRef]
58. Yunarti, R.T.; Gu, S.; Choi, J.-W.; Jae, J.; Suh, D.J.; Ha, J.-M. Oxidative coupling of methane using Mg/Ti-doped SiO_2-supported Na_2WO_4/Mn Catalysts. *ACS Sustain. Chem. Eng.* **2017**, *5*, 3667–3674. [CrossRef]
59. Ghose, R.; Hwang, H.T.; Varma, A. Oxidative coupling of methane using catalysts synthesized by solution combustion method. *Appl. Catal. A Gen.* **2013**, *452*, 147–154. [CrossRef]
60. Yildiz, M.; Aksu, Y.; Simon, U.; Kailasam, K.; Goerke, O.; Rosowski, F.; Schomäcker, R.; Thomas, A.; Arndt, S. Enhanced catalytic performance of Mn_xO_y–Na_2WO_4/SiO_2 for the oxidative coupling of methane using an ordered mesoporous silica support. *Chem. Commun.* **2014**, *50*, 14440–14442. [CrossRef]
61. Li, S.-B. Oxidative Coupling of Methane over W-Mn/SiO_2 Catalyst. *Chin. J. Chem.* **2001**, *19*, 16–21. [CrossRef]
62. Wang, D.J.; Rosynek, M.P.; Lunsford, J.H. Oxidative Coupling of Methane over Oxide-Supported Sodium-Manganese Catalysts. *J. Catal.* **1995**, *155*, 390–402. [CrossRef]
63. Sofranko, J.A.; Leonard, J.J.; Jones, C.A.; Gaffney, A.M.; Withers, H.P. Catalytic oxidative coupling of methane over sodium-promoted Mn/SiO_2 and Mn/MgO. *Catal. Today* **1988**, *3*, 127–135. [CrossRef]
64. Ortiz-Bravo, C.A.; Figueroa, S.J.A.; Portela, R.; Chagas, C.A.; Bañares, M.A.; Toniolo, F.S. Elucidating the structure of the W and Mn sites on the Mn-Na_2WO_4/SiO_2 catalyst for the oxidative coupling of methane (OCM) at real reaction temperatures. *J. Catal.* **2021**. [CrossRef]

65. Xueping, F.; Shuben, L.; Jingzhi, L.; Yanlai, C. Oxidative coupling of methane on W-Mn catalysts. *J. Mol. Catal. China* **1992**, *6*, 427–433.
66. Lee, J.Y.; Jeon, W.; Choi, J.-W.; Suh, Y.-W.; Ha, J.-M.; Suh, D.J.; Park, Y.-K. Scaled-up production of C_2 hydrocarbons by the oxidative coupling of methane over pelletized $Na_2WO_4/Mn/SiO_2$ catalysts: Observing hot spots for the selective process. *Fuel* **2013**, *106*, 851–857. [CrossRef]
67. Hayek, N.S.; Khlief, G.J.; Horani, F.; Gazit, O.M. Effect of reaction conditions on the oxidative coupling of methane over doped MnOx-Na_2WO_4/SiO_2 catalyst. *J. Catal.* **2019**, *376*, 25–31. [CrossRef]
68. Jeon, W.; Lee, J.Y.; Lee, M.; Choi, J.-W.; Ha, J.-M.; Suh, D.J.; Kim, I.W. Oxidative coupling of methane to C_2 hydrocarbons on the Mg–Ti mixed oxide-supported catalysts at the lower reaction temperature: Role of surface oxygen atoms. *Appl. Catal. A Gen.* **2013**, *464–465*, 68–77. [CrossRef]
69. Wang, H.; Schmack, R.; Paul, B.; Albrecht, M.; Sokolov, S.; Rümmler, S.; Kondratenko, E.V.; Kraehnert, R. Porous silicon carbide as a support for Mn/Na/W/SiC catalyst in the oxidative coupling of methane. *Appl. Catal. A Gen.* **2017**, *537*, 33–39. [CrossRef]
70. Colmenares, M.G.; Simon, U.; Yildiz, M.; Arndt, S.; Schomaecker, R.; Thomas, A.; Rosowski, F.; Gurlo, A.; Goerke, O. Oxidative coupling of methane on the Na_2WO_4-MnxOy catalyst: COK-12 as an inexpensive alternative to SBA-15. *Catal. Commun.* **2016**, *85*, 75–78. [CrossRef]
71. Wu, J.; Zhang, H.; Qin, S.; Hu, C. La-promoted $Na_2WO_4/Mn/SiO_2$ catalysts for the oxidative conversion of methane simultaneously to ethylene and carbon monoxide. *Appl. Catal. A Gen.* **2007**, *323*, 126–134. [CrossRef]
72. Chou, L.; Cai, Y.; Zhang, B.; Niu, J.; Ji, S.; Li, S. Influence of SnO_2-doped W-Mn/SiO_2 for oxidative conversion of methane to high hydrocarbons at elevated pressure. *Appl. Catal. A Gen.* **2003**, *238*, 185–191. [CrossRef]
73. Shahri, S.M.K.; Pour, A.N. Ce-promoted Mn/Na_2WO_4/SiO_2 catalyst for oxidative coupling of methane at atmospheric pressure. *J. Nat. Gas Chem.* **2010**, *19*, 47–53. [CrossRef]
74. Sun, W.; Gao, Y.; Zhao, G.; Si, J.; Liu, Y.; Lu, Y. Mn_2O_3-Na_2WO_4 doping of $Ce_xZr_{1-x}O_2$ enables increased activity and selectivity for low temperature oxidative coupling of methane. *J. Catal.* **2021**, *400*, 372–386. [CrossRef]
75. Kim, G.J.; Ausenbaugh, J.T.; Hwang, H.T. Effect of TiO_2 on the Performance of Mn/Na_2WO_4 Catalysts in Oxidative Coupling of Methane. *Ind. Eng. Chem. Res.* **2021**, *60*, 3914–3921. [CrossRef]
76. Ji, S.; Xiao, T.; Li, S.; Chou, L.; Zhang, B.; Xu, C.; Hou, R.; York, A.P.E.; Green, M.L.H. Surface WO_4 tetrahedron: The essence of the oxidative coupling of methane over M–W–Mn/SiO_2 catalysts. *J. Catal.* **2003**, *220*, 47–56. [CrossRef]
77. Xu, J.; Peng, L.; Fang, X.; Fu, Z.; Liu, W.; Xu, X.; Peng, H.; Zheng, R.; Wang, X. Developing reactive catalysts for low temperature oxidative coupling of methane: On the factors deciding the reaction performance of $Ln_2Ce_2O_7$ with different rare earth A sites. *Appl. Catal. A Gen.* **2018**, *552*, 117–128. [CrossRef]
78. Xu, J.; Zhang, Y.; Xu, X.; Fang, X.; Xi, R.; Liu, Y.; Zheng, R.; Wang, X. Constructing $La_2B_2O_7$ (B = Ti, Zr, Ce) Compounds with Three Typical Crystalline Phases for the Oxidative Coupling of Methane: The Effect of Phase Structures, Superoxide Anions, and Alkalinity on the Reactivity. *ACS Catal.* **2019**, *9*, 4030–4045. [CrossRef]
79. Zhang, Y.; Xu, J.; Xu, X.; Xi, R.; Liu, Y.; Fang, X.; Wang, X. Tailoring $La_2Ce_2O_7$ catalysts for low temperature oxidative coupling of methane by optimizing the preparation methods. *Catal. Today* **2020**, *355*, 518–528. [CrossRef]
80. Xu, J.; Xi, R.; Xu, X.; Zhang, Y.; Feng, X.; Fang, X.; Wang, X. $A_2B_2O_7$ pyrochlore compounds: A category of potential materials for clean energy and environment protection catalysis. *J. Rare Earths* **2020**, *38*, 840–849. [CrossRef]
81. Petit, C.; Rehspringer, J.L.; Kaddouri, A.; Libs, S.; Poix, P.; Kiennemann, A. Oxidative coupling of methane by pyrochlore oxide $A_2B_2O_7$ (A = rare earth, B = Ti, Zr, Sn). Relation between C_2 selectivity and B–O bond energy. *Catal. Today* **1992**, *13*, 409–416. [CrossRef]
82. Zhang, F.X.; Tracy, C.L.; Lang, M.; Ewing, R.C. Stability of fluorite-type $La_2Ce_2O_7$ under extreme conditions. *J. Alloy Compd.* **2016**, *674*, 168–173. [CrossRef]
83. Wang, Z.; Zhou, G.; Jiang, D.; Wang, S. Recent development of $A_2B_2O_7$ system transparent ceramics. *J. Adv. Ceram.* **2018**, *7*, 289–306. [CrossRef]
84. Modeshia, D.R.; Walton, R.I. Solvothermal synthesis of perovskites and pyrochlores: Crystallisation of functional oxides under mild conditions. *Chem. Soc. Rev.* **2010**, *39*, 4303–4325. [CrossRef] [PubMed]
85. Xu, J.; Zhang, Y.; Liu, Y.; Fang, X.; Xu, X.; Liu, W.; Zheng, R.; Wang, X. Optimizing the reaction performance of $La_2Ce_2O_7$-based catalysts for oxidative coupling of methane (OCM) at lower temperature by lattice doping with Ca cations. *Eur. J. Inorg. Chem.* **2019**, *2019*, 183–194. [CrossRef]
86. Mims, C.A.; Jacobson, A.J.; Hall, R.B.; Lewandowski, J.T. Methane oxidative coupling over nonstoichiometric bismuth-tin pyrochlore catalysts. *J. Catal.* **1995**, *153*, 197–207. [CrossRef]
87. Roger, A.C.; Petit, C.; Kiennemann, A. Effect of metallo-organic precursors on the synthesis of Sm–Sn pyrochlore catalysts: Application to the oxidative coupling of methane. *J. Catal.* **1997**, *167*, 447–459. [CrossRef]
88. Ashcroft, A.T.; Cheetham, A.K.; Green, M.L.H.; Grey, C.P.; Vernon, P.D.F. Oxidative coupling of methane over tin-containing rare-earth pyrochlores. *J. Chem. Soc. Chem. Commun.* **1989**, 1667–1669. [CrossRef]
89. Wu, G.; Murthy, P.R.; Chen, B.; Zhang, X.; Shi, C.; Guo, X.; Song, C. Investigation on Sr doped $La_2Ce_2O_7$ pyrochlore as effective catalyst for oxidative coupling of methane. *Mod. Chem. Ind.* **2021**. [CrossRef]